Analysis of acoustic impedance matching in dual-band ultrasound transducers

Ola Finneng Myhre, Tonni Franke Johansen, and Bjørn Atle Johan Angelsen

Citation: The Journal of the Acoustical Society of America **141**, 1170 (2017); doi: 10.1121/1.4976096
View online: http://dx.doi.org/10.1121/1.4976096
View Table of Contents: http://asa.scitation.org/toc/jas/141/2
Published by the Acoustical Society of America

Analysis of acoustic impedance matching in dual-band ultrasound transducers

Ola Finneng Myhre,[a] Tonni Franke Johansen,[b] and Bjørn Atle Johan Angelsen
Department of Circulation and Medical Imaging, Norwegian University of Science and Technology, P.O. Box 8905, N-7489 Trondheim, Norway

(Received 16 November 2016; revised 16 January 2017; accepted 19 January 2017; published online 28 February 2017)

Dual-frequency band probes are needed for ultrasound (US) reverberation suppression and are useful for image-guided US therapy. A challenge is to design transducer stacks that achieve high bandwidth and efficiency at both operating frequencies when the frequencies are widely separated with a frequency ratio ~6:1–20:1. This paper studies the loading and backing conditions of transducers in such stacks. Three stack configurations are presented and analyzed using one-dimensional models. It is shown that a configuration with three layers of material separating the transducers is favorable, as it reduces high frequency ringing by ~20 dB compared to other designs, and matches the low frequency (LF) transducer to the load at a lower frequency. In some cases, the LF load matching is governed by a simple mass–spring interaction in spite of having a complicated matching structure. The proposed design should yield improved performance of reverberation suppression algorithms. Its suitability for reduction of probe heating, also in single-band probes, should be investigated. © *2017 Acoustical Society of America*. [http://dx.doi.org/10.1121/1.4976096]

[JFL] Pages: 1170–1179

I. INTRODUCTION

Second order UltRasound Field (SURF) imaging[1,2] is a dual-band ultrasound imaging method that requires the simultaneous transmission of overlapping pulses at widely separated frequencies. A high frequency (HF) imaging pulse co-propagates with a low frequency (LF) manipulation pulse. In medical applications, the HF may be ~2–20 MHz, whereas the LF may be ~0.3–2 MHz. The HF pulse alters the propagation velocity of the HF pulse,[2] and it also alters how the HF pulse is scattered by non-linear scatterers.[2,3] The HF-to-LF ratio is typically $\chi_R \sim 6{:}1–20{:}1$. Dual-band transducers with such a ratio are potentially also useful for combined ultrasound imaging and therapy, as the latter may also require the transmission of ultrasound at widely spaced frequencies.[4]

Piezoelectric transducers are most efficient when driven at resonance, so an ultrasound probe producing pulses with widely separated frequencies should contain two transducers—one for each operating band. SURF probes, therefore, contain two transducers in a stacked configuration, so that the LF pulse is transmitted through the HF transducer. The stack design comprises three sections, as shown in Fig. 1: (i) the HF section, (ii) the isolation section, and (iii) the LF section, each of which may contain multiple layers of material. The purpose of the isolation section is to prevent transmission of HF pulses into the LF section and to match the LF section of the probe to the load. The challenge is to design an isolation section which minimizes HF ringing and matches the LF section to the load, irrespective of the HF-to-LF ratio. This paper presents three isolation section configurations and investigates their effect on the HF and LF performance of a SURF imaging probe. It also aims to give a physical understanding of the design, and to provide guidelines for designing SURF probes, akin to those developed for single-band probes.[5] Similar designs have been described with HF-to-LF frequency ratios of 2:1, for the purpose of optimizing transducers for B-mode[6] and Doppler color flow[7] imaging in medical ultrasound.

The SURF method is used for reverberation suppression[8,9] and imaging of non-linear scatterers at high frequencies.[3,10] Its usefulness in estimating tissue elasticity parameters is currently also under investigation.[11] In each of these applications, it is advantageous to have a large HF-to-LF ratio, and to have continuous overlap of the HF and LF transmission fields within the HF imaging region. The HF-to-LF ratio cannot be increased indefinitely. As the LF is decreased, the LF aperture must be increased to ensure that the LF pressure is maximally spatially invariant across the wave front of the HF pulse.[12] Decreasing the LF also increases the mechanical index (MI) of the transmitted LF field. SURF reverberation suppression requires that the LF pressure is sufficiently large in order to minimize electronic noise in the post-processed image. For a certain LF pressure requirement, the upper bound on the HF-to-LF ratio may be limited by MI. It is, therefore, important to be able to tailor the HF-to-LF ratio without affecting the HF performance.

As opposed to tissue harmonic imaging (THI) or pulse inversion (PI), which utilize the second harmonic in the received signal(s) to suppress reverberation noise, SURF imaging may suppress reverberations by considering only the fundamental band. SURF probes may, therefore, have narrower HF band than probes which are used for THI or PI. However, large HF bandwidth is still required to have high

[a]Also at: Kreftklinikken, St. Olavs Hospital HF, P.O. Box 3250 Sluppen, 7006 Trondheim, Norway. Electronic mail: ola.f.myhre@ntnu.no
[b]Also at: SINTEF Information and Communication Technology (ICT), Acoustics, P.O. Box 4760 Sluppen, N-7465 Trondheim, Norway.

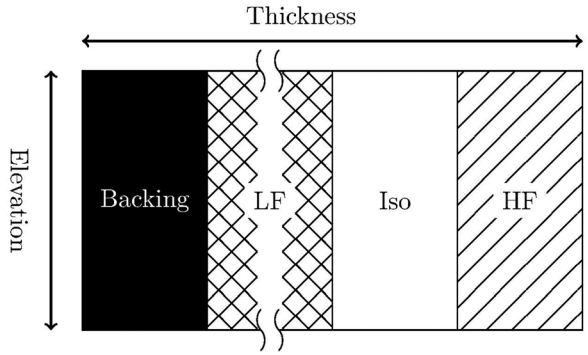

FIG. 1. Cross-sectional view of the structure of the transducer stack. From left to right, the stack consists of a backing, a low frequency section, an isolation section, and a HF section. Note that the illustration of the stack is not to scale, and that each of the sections may consist of multiple layers of materials.

radial resolution. Large HF bandwidth is also necessary in order to achieve high suppression of reverberations in SURF processing. Shorter HF pulses are distorted less by the presence of the LF pulse since the LF pressure varies less over the length of shorter HF pulses compared to longer HF pulses. A long HF pulse will counteract the benefit of having a large HF-to-LF ratio.

This paper focuses on how the HF backing impedance and the LF loading impedance are affected by different isolation section configurations. Due to the large HF-to-LF ratio, the loading condition of the LF transducer is modeled using one-dimensional lumped parameter models, whereas the HF backing impedance is modeled with a one-dimensional distributed model. The lumped models help to quantify and understand how and why stack parameters affect the LF transducer performance as they are simpler to analyze mathematically. For completeness and self-containment, an overview of the distributed and lumped models is presented in Sec. II, along with the lumped parameter model error relative to the distributed model. Readers who are well-versed in acoustic theory may consider skipping Sec. II and proceeding to Sec. III, where the models are used to analyze and compare three isolation section configurations.

II. WAVE PROPAGATION MODELS

Figure 1 shows the structure of the stack in the dual-band probe. Within each section, each layer of material is a plate with lateral dimensions that are much larger than the thickness of the plate. Each plate can be analyzed with a one-dimensional model of wave propagation, using either a distributed model or a lumped parameter model. The distributed model is a powerful tool for performing stack simulations, but is more difficult to use for analytic discussion. At lower frequency, the lumped models provide an approximate description of the stack, and are more suited for analysis. An overview of the models is given before investigating different isolation layer configurations. Note that in this paper, the specific acoustic impedance is referred to simply as acoustic impedance.

A. Distributed models

The distributed model for vibration in a material is constructed from considering compressional pressure waves that propagate backwards and forwards in the stack. The resulting representation of the plate is analogous with the representation of a transmission line. The characteristic impedance of the transmission line is in the acoustic model analogous to the characteristic impedance of the plate material, $Z_0 = \sqrt{\rho_0/\kappa_0}$, where ρ_0 is the mass density and κ_0 is the bulk compressibility. In the acoustic case, voltage is replaced by pressure, p, and current by vibration velocity, u.[13]

The acoustic impedance seen through a plate into an arbitrary load is an important quantity in stack analysis. Let the characteristic impedance of the plate be Z_0 and its thickness d_0. Let ω be the angular frequency and the acoustic impedance of the structure loading the plate be $Z_R = Z_R(\omega)$. When $\gamma = \gamma(\omega) = \alpha(\omega) + \jmath\beta(\omega)$ is the propagation constant of the material, the acoustic input impedance is[13]

$$Z_D^F(\omega) = Z_0 \frac{Z_R \cosh(d_0\gamma) + Z_0 \sinh(d_0\gamma)}{Z_0 \cosh(d_0\gamma) + Z_R \sinh(d_0\gamma)}, \tag{1}$$

where the subscript D indicates that a distributed model is used for the plate, and superscript F denotes that the impedance is considered forwards through the plate.

In a lossless, non-dispersive material, $d_0\gamma(\omega) = \jmath\beta(\omega)d_0 = \jmath\omega d_0/c_0 = 2\pi\jmath d_0/\lambda$, where λ is the wavelength of the wave and c_0 is propagation speed in the medium.

In general, the loading impedance $Z_R(\omega)$ is complex. However, when the plate is loaded by a semi-infinite medium, the loading impedance is simply the characteristic impedance of the loading medium, a real constant. In this case, neglecting losses, the absolute value of Eq. (1) has critical points in $d_0/\lambda = n/4$, $n = 1, 2, \ldots$, in which the function values are

$$|Z_D^F(n)| = \begin{cases} Z_0^2/Z_R, & n \text{ odd} \\ Z_R, & n \text{ even}. \end{cases} \tag{2}$$

When considering the acoustic impedance of many plates that are stacked on top of one another, Eq. (1) is cascaded, leading to a complicated expression that is difficult to evaluate analytically.

The transmission line can be represented by a T-model, shown in Fig. 2, or by a Π-model, shown in Fig. 3, where both are useful for making approximations at low frequencies.

B. Lumped parameter models

When the thickness of the plate is small compared to the wavelength, the hyperbolic functions in the T- and Π-models can be approximated by first order polynomials. The thickness of the plate, d_0, can be written as a fraction of the wavelength at a reference frequency f_0, so that

$$d_0 = \nu_0 \frac{c_0}{f_0} = \nu_0 \lambda_0. \tag{3}$$

In the lossless, non-dispersive case, the plate is approximated by two inductors and a capacitor, as shown in the

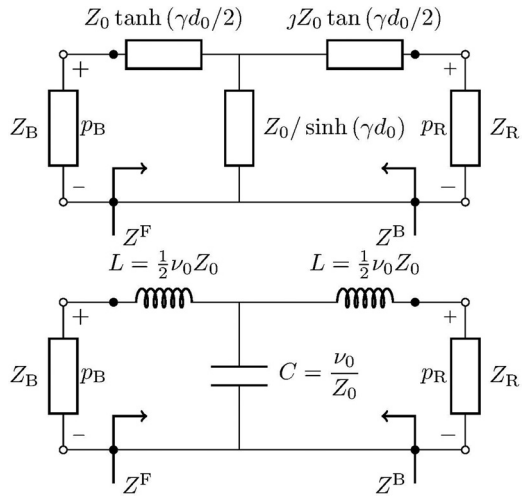

FIG. 2. T-model equivalent circuit for a resonant slab of material, represented with a distributed (top) and lumped (bottom) model. The subscript R indicates the loading material, and subscript B indicates the backing material. The superscript F denotes the impedance which is seen forwards, towards the load side of the plate, at a certain point. The superscript B denotes the impedance which is seen backwards, towards the backing side of the plate, at a certain point.

bottom panels of Figs. 2 and 3. The hyperbolic components of the top panels simplify to

$$\tanh(\gamma d_0/2) = \jmath \tan(\pi d_0/\lambda) \approx \nu_0 \jmath \pi \omega/\omega_0, \tag{4}$$

$$\sinh(\gamma d_0) = \jmath \sin(2\pi d_0/\lambda) \approx \nu_0 \jmath 2\pi \omega/\omega_0, \tag{5}$$

so that the values of the reactive components in the two models are

$$L = \frac{1}{2} L_\Pi = \frac{\pi\omega}{\omega_0}\nu_0 Z_0, \tag{6}$$

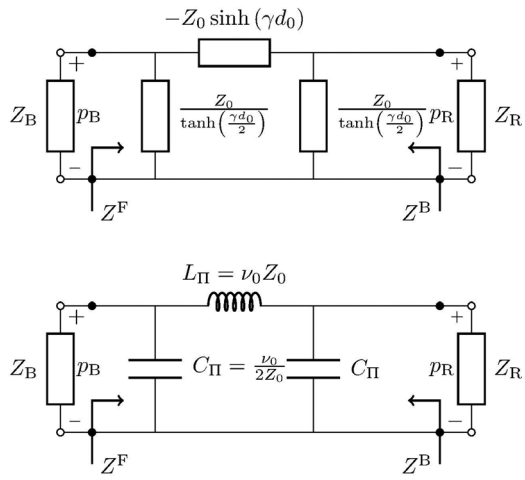

FIG. 3. Π-model equivalent circuit for a resonant slab of material, represented with a distributed (top) and lumped (bottom) model. The subscript R indicates the loading material, and subscript B indicates the backing material. The superscript F denotes the impedance which is seen forwards, towards the load side of the plate, at a certain point. The superscript B denotes the impedance which is seen backwards, towards the backing side of the plate, at a certain point.

$$C = 2C_\Pi = \frac{2\pi}{\omega_0}\frac{\nu_0}{Z_0}. \tag{7}$$

The inductance in Eq. (6) depends on the mass per unit area of the plate, whereas the capacitance in Eq. (7) is inversely proportional to the compliance of the plate. These are valid models when the thickness of the material is small compared to the wavelength of the vibrations.[14] The acoustic input impedance of a T-model with a loading impedance $Z_L(\omega)$ is

$$Z_T^F(\omega) = \frac{Z_{RB}(\omega) + Z_R(\omega)}{Z_C(\omega) + Z_{RB}(\omega) + Z_R(\omega)} Z_{LB}(\omega) + \frac{Z_{LB}(\omega) + Z_{RB}(\omega) + Z_R(\omega)}{Z_C(\omega) + Z_{RB}(\omega) + Z_R(\omega)} Z_C(\omega), \tag{8}$$

where $Z_{LB}(\omega)$ and $Z_{RB}(\omega)$ are the impedances in the left and right branches of the T-model, respectively. $Z_C(\omega)$ is the shunt impedance. Using Eq. (8), two special cases may be noted. Let $\Im\{\cdot\}$ denote taking the imaginary component of a complex number. When $Z_{LB}(\omega) \ll Z_C(\omega)$ and $\Im\{Z_{LB}(\omega) + Z_{RB}(\omega)\} \ll \Im\{Z_R(\omega)\}$, the plate may be approximated by a single capacitor. Equation (8) reduces to

$$Z_T^F(\omega) \approx \frac{Z_R(\omega)}{Z_C(\omega) + Z_R(\omega)} Z_C(\omega), \tag{9}$$

which is the expression describing the impedance of $Z_C(\omega)$ and $Z_R(\omega)$ connected in parallel. When $Z_{LB}(\omega) \ll Z_C(\omega)$ and $|Z_C(\omega)| \gg |[Z_{RB}(\omega) + Z_R(\omega)]|$, the plate may be approximated by a single inductor. Equation (8) reduces to

$$Z_T^F(\omega) \approx Z_{LB}(\omega) + Z_{RB}(\omega) + Z_R(\omega), \tag{10}$$

which is the expression describing the impedance of $Z_{LB}(\omega)$, $Z_{RB}(\omega)$, and $Z_R(\omega)$ connected in series. Using Eqs. (6) and (7) to express $Z_{LB}(\omega)$ and $Z_C(\omega)$ for the lumped model, it is found that the common requirement for these special cases, $Z_{LB}(\omega) \ll Z_C(\omega)$, also implies

$$Z_{LB}(\omega) \ll Z_C(\omega) \rightarrow \omega^2 \ll \frac{1}{2}\left(\frac{\omega_0}{\pi\nu_0}\right)^2. \tag{11}$$

The second requirement for modeling the plate using a single capacitor is generally true when the reactive component of $Z_R(\omega)$ is inductive and larger than the inductive component of the plate,

$$2\pi\omega\nu_0 Z_0/\omega_0 \ll \Im\{Z_R(\omega)\}, \tag{12}$$

meaning that the load is more massive than the plate. Interpreting the second requirement for modeling the plate an inductor is more involved since, in general, $Z_R(\omega)$ is a complex quantity. However, imposing the stricter requirement that $|Z_{RB}(\omega)| + |Z_R(\omega)| \ll Z_C(\omega)$, results in the requirement that

$$|Z_R(\omega)| \ll Z_0 \frac{\omega_H}{2\pi\nu_0\omega}\left[1 - \frac{1}{2}\left(\frac{2\pi\nu_0\omega}{\omega_H}\right)^2\right], \tag{13}$$

which, by applying the requirement in Eq. (11), simplifies to

$$|Z_R(\omega)| \ll Z_0 \frac{\omega_H}{2\pi\nu_0\omega} = |Z_C(\omega)|. \quad (14)$$

In summary, thin plates of stiff or dense material, with a high characteristic impedance, can be modeled as masses when the loading impedance is low. Thin plates of compliant or light materials, with low characteristic impedance, are well approximated as springs when the loading impedance is high. Examples of the model error are shown in Fig. 4 for $|\alpha| = |Z_R(\omega)/Z_0| = 1$ and $\nu_0 = 0.5$. Note that the errors decrease as ν_0 is decreased. Furthermore the error in the capacitor model decreases as $|\alpha|$ is increased, whereas the inductor model error increases as $|\alpha|$ is decreased. The Π-filter model in Fig. 3 has approximately the same performance as the T-model in Fig. 2. Having all of the above models available is useful when modeling and performing mathematical analysis of a transducer stack.

III. ISOLATION SECTION ANALYSIS

The configuration of the layers in the isolation section of the stack is investigated with the mathematical tools from Sec. II. The purpose of the isolation section is to (i) minimize the amount of HF ringing due to multiple reflections within the LF and isolation sections, and (ii) to optimize the loading conditions of the LF transducer.

A. Configurations

Sections III B and III C show how the three different isolation section configurations, shown in Fig. 5, affect the HF and LF transducers. In the analysis, the layers are enumerated from front to back, as shown in Fig. 5, with layers 1 and 2 denoting two matching layers in front of the HF transducer, which is layer number 3. The isolation layers are the fourth, fifth, and sixth layers of the stack, and the parameters of each layer are enumerated accordingly. Layer 7 denotes the LF transducer, whereas layer 8 is the backing.

B. HF Transmit performance

When investigating the effect that the isolation section structure has on HF performance, it is necessary to use the distributed model of the layers, i.e., Eq. (1), since they have thicknesses that are comparable to the HF wavelength, and Eqs. (4) and (5) do not hold. The HF transmit performance is evaluated by using Eq. (1) and the Mason model[15] for piezoelectric transducers. In the simulation, a voltage with a Gaussian envelope is applied to the HF piezoelectric layer. The vibration velocity on the transducer surface is recorded, and shown for the three stack configurations in Fig. 6. The full list of parameters for the simulations is given in Table I.

The isolation section should eliminate spurious transmit pulses that occur due to reflections of the HF pulse in the layers behind the HF transducer. In the one-dimensional model, this can be achieved by adjusting the backing condition of the HF transducer so that total reflection is achieved at the back face of the HF transducer.

In SURF probes, the LF section acts as a semi-infinite medium when determining the effective backing impedance in the HF band since the HF pulse length is less than the thickness of the LF section. The LF section also typically has a high impedance. This means that the backing impedance for the isolation section is large at HF. Since the HF backing impedance should be minimized, the isolation section should have the property of being a quarter-wave impedance transformer at HF. Letting the isolation section be a series of k quarter-wave transformers with $\nu_k = 0.25$ the HF backing impedance at the HF angular center frequency, ω_H, can be calculated from Eq. (1) as

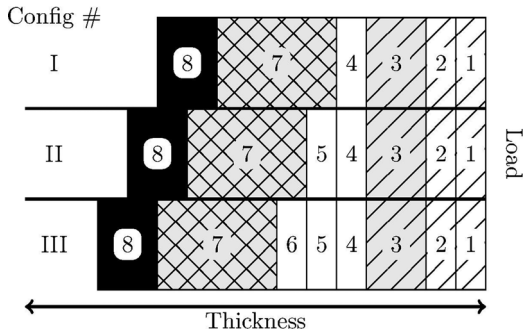

FIG. 5. Isolation section configurations considered in this paper. The backing is shown in black, and the transducers are gray. The layers of the LF section are shown with a grid pattern, whereas the layers in the HF section are shown with a line pattern. The isolation section layers are shown in white, without patterning.

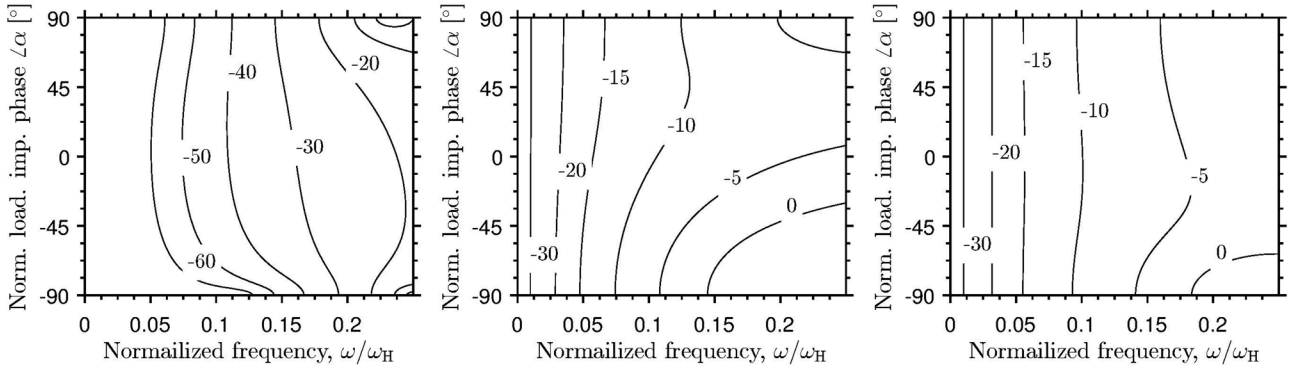

FIG. 4. The error in the T-section (left), capacitor (middle), and inductor (right) models relative to the distributed model. The relative error is given in decibels, with normalized frequency on the abscissa, and the phase of the normalized loading impedance on the ordinate. The fractional thickness of the plate is $\nu_0 = 0.5$ and the normalized load impedance magnitude is $|\alpha| = 1$.

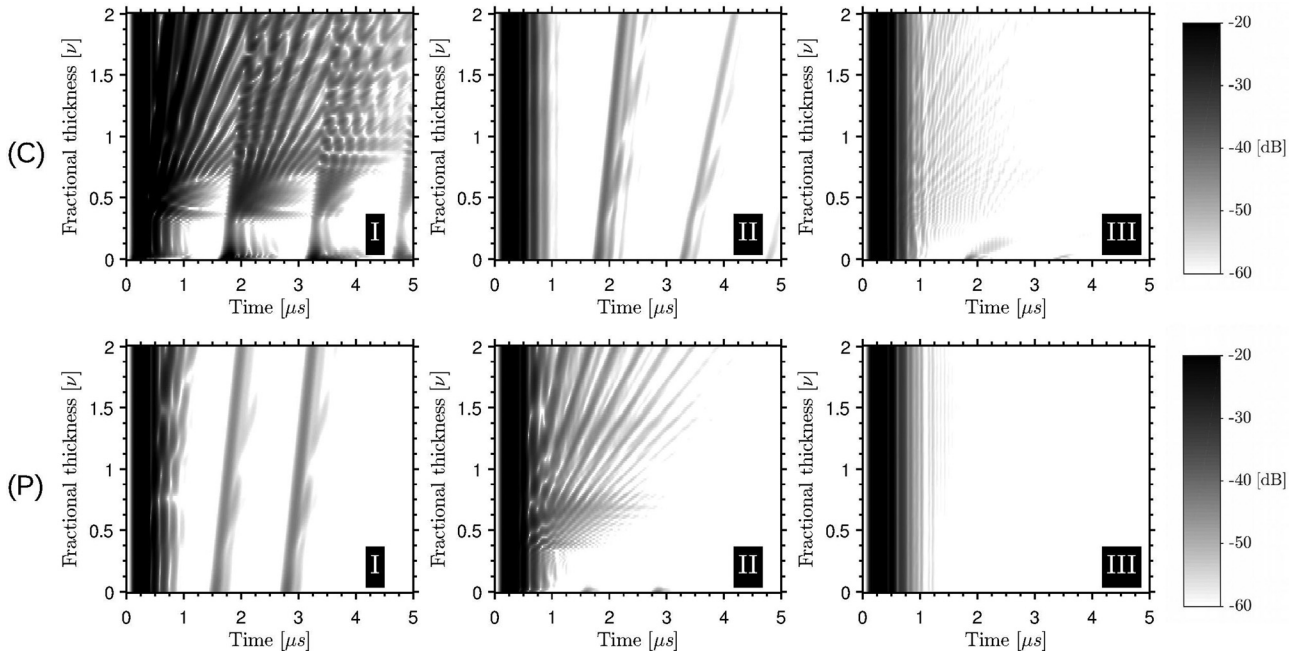

FIG. 6. Simulations of HF transmissions when using different configurations (I, II, III), when the LF transducer is purely ceramic (C), $Z_L = 35$ MRayl, or purely polymeric (P), $Z_L = 3.0$ MRayl. The excitation is a Gaussian pulse with center frequency ω_H and a relative bandwidth of 75%. The envelopes of the transmit wave forms are shown in the decibel scale. The ordinate shows the variation in fractional thickness of the rear isolation layer in each case. Parameters for each case are (I) $Z_4 = 2.34$ MRayl, ν_4 varied; (II) $Z_4 = 2.34$ MRayl, $Z_5 = 44.5$ MRayl, $\nu_4 = 0.25$, ν_5 varied; (III) $Z_4 = 2.34$ MRayl, $Z_5 = 44.5$ MRayl, $Z_6 = 2.34$ MRayl, $\nu_4 = \nu_5 = 0.25$, ν_6 varied. All layers have an acoustic quality factor of $Q = 50$.

$$Z^{B}_{Hk}(\omega_H) = \begin{cases} \dfrac{Z_L \prod_{i=1}^{k/2} Z^2_{(2i-1+\sigma)}}{\prod_{i=1}^{k/2} Z^2_{(2i+\sigma)}}, & k \text{ even} \\ \dfrac{\prod_{i=1}^{(k+1)/2} Z^2_{(2i-1+\sigma)}}{Z_L \prod_{i=1}^{(k-1)/2} Z^2_{(2i+\sigma)}}, & k \text{ odd} \end{cases} \quad (15)$$

where the numeric subscripts of Z denote the layer number, in accordance with the numeration in Fig. 5, and σ is the number of layers in the HF section. Since Z_L is large, and the HF backing impedance should be low, Eq. (15) shows that an odd number of isolation layers is the natural choice for achieving good isolation for the HF transducer. With low impedance in each odd-numbered layer, and high impedance in each even-numbered layer, the backing impedance will be low at HF.

In SURF transducers, HF and LF elements may not be perfectly aligned, meaning that any given HF element could either be positioned in front of an LF element, or in front of the kerf in between LF elements. Z_L is high or low, respectively, in these cases. A design which mitigates the effect of variation in Z_L on the HF backing impedance is needed to ensure that the HF performance is not affected by the relative positions of the HF and LF elements.

1. Configuration I

With a single isolation layer, the HF backing impedance at the HF center frequency is minimum when selecting $\nu_4 \approx 0.25$, while the characteristic impedance of the isolation layer is low. Z_4 is the characteristic impedance of the first isolation layer, and Z_L is the characteristic impedance of the LF section. Equation (15) gives the HF backing impedance with configuration I ($k = 1$),

$$Z^{B}_{H1}(\omega_H) = \frac{Z_4^2}{Z_L}. \quad (16)$$

Figure 6 (CI) and (PI) show how configuration I produces spurious HF transmit pulses, with amplitudes approximately –20 to –30 dB relative to the amplitude of the main HF transmission pulse. The spurious pulses originate from the back of the LF section, irrespective of the LF section impedance, as shown by the 1.5 μs periodicity in Fig. 6 (CI) and (PI). With a large Z_L, there are also multiple reflections within the isolation layer, particularly for $\nu_4 > 1$, which is shown by the rapid variations in Fig. 6 (PI). The simulations show that the thickness of the first isolation layer should be $\nu_4 \approx 0.25$ in order to minimize reflections within the isolation layer. Furthermore, the amplitudes of the spurious HF transmissions are significant with configuration I.

2. Configuration II

Increasing the number of isolation layers to two as in configuration II can homogenize the HF backing impedance so that the variation in the effective impedance of the LF section has less of an impact on the HF backing impedance.[16] Figure 7 shows an example of how the addition of the second isolation layer homogenizes the HF backing impedance with $\nu_4 = \nu_5 = 0.25$ and $Z_5 \gg Z_4$.

With two quarter-wave transformers,

$$Z^{\mathrm{B}}_{\mathrm{H2}}(\omega_{\mathrm{H}}) = \frac{Z_4^2}{Z_5^2} Z_{\mathrm{L}}. \tag{17}$$

Although $Z^B_{H2}(\omega_H) \propto Z_L$, the variation of Z_L is mitigated by a scaling factor $(Z_4/Z_5)^2$, which is low if $Z_5 \gg Z_4$. However, the difference in the impedance of the second isolation layer and the LF section ceramic is not large, so waves are transmitted through and reflect off the back of the LF section. This explains the presence of spurious HF transmissions seen in Fig. 7 (CII). With a low Z_L, there is close to total reflection behind the second isolation layer, and the amplitudes of the rapid spurious HF transmissions originating from the first isolation layer are negligible, as shown in Fig. 7 (PII). However, as the thickness of the second isolation layer is increased, it becomes resonant in the HF band, and produces more spurious HF transmissions, as shown by the rapid variation in Fig. 7 (PII). Again, in order to minimize the amount of spurious HF transmissions, the thickness of the second isolation layer should be selected so that $\nu_5 \approx 0.25$, and the characteristic impedance should be $Z_5 > Z_L$.

3. Configuration III

Figure 6 (CI), (CII), (PI), and (PII) show that the first and second isolation layers have optimal fractional thicknesses of $\nu_4 \approx \nu_5 \approx 0.25$. Even using these optimal thicknesses, when Z_L is large there are still spurious HF transmissions with amplitudes of –20 to –40 dB relative to the amplitude of the main HF transmission pulse. Being in front of the LF section, the isolation layers have a part in determining the LF matching. Since relatively small variations in the thickness and characteristic impedance of these layers strongly affect HF performance, these configurations offer little flexibility in tuning matching for the LF section. The lack of flexibility and persistent presence of spurious HF transmissions therefore makes it interesting to examine how a third isolation layer affects the HF performance.

From Eq. (15), configuration III ($k = 3$) yields an HF backing impedance

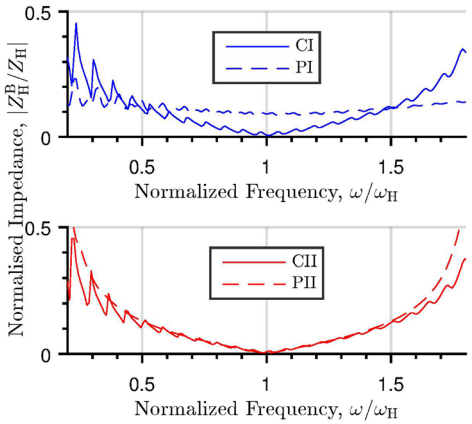

FIG. 7. (Color online) The HF backing impedance with configurations I and II. $Z_4 = 2.34$ MRayl, $Z_4 = 44.5$ MRayl, $\nu_4 = \nu_5 = 0.25$, and the LF layer has $Z_{\mathrm{L}} = 3.0$ MRayl (P) or $Z_{\mathrm{L}} = 35$ MRayl (C).

$$Z^B_{H3}(\omega_H) = \frac{Z_4^2 Z_6^2}{Z_5^2 Z_L}. \tag{18}$$

By selecting a low impedance material for the third isolation layer, the backing impedance becomes very low, since $Z_5^2 \gg (Z_4 Z_6)^2$ and $Z^B_{H3}(\omega_H) \propto 1/Z_L < 1$. Figure 6 (CIII) and (PIII) shows varying the thickness of the third isolation layer affects HF transmission. The amplitudes of the spurious transmissions are reduced to –60 to –55 dB relative to the amplitude of the main HF transmission pulse, and the change is relatively constant with respect to the thickness of the layer. When the thickness of the layer is small compared to the HF pulse length the reflections from each interface in the isolation section interfere so that the effective backing impedance is given by Eq. (18). Conversely, when the thickness is large compared to the pulse length, the reflection from the interface between the third isolation layer and the LF section does not interfere with reflections from the other interfaces in the isolation section. The effective backing impedance is therefore given by

$$Z^B_{H3}(\omega_H) = \frac{Z_4^2}{Z_5^2 Z_6}. \tag{19}$$

With $Z_6 \sim Z_4$, the effective backing impedance is given by the ratio Z_4/Z_5^2, which is small since $Z_5 > Z_4$.

C. LF load matching

All the layers in front of the LF transducer have thicknesses that are a fraction of the HF wavelength. Furthermore, the HF-to-LF ratio is large, so Eqs. (4) and (5) hold in the LF band. Lumped models are therefore used to study the effect of the isolation layers on the LF transducer.

1. Assumptions

With reference to Fig. 5 the HF section of the probe contains two matching layers and a transducer operating at half-wave resonance. The characteristic impedances of the layer are increasing from the loading material to the HF transducer; $Z_R < Z_1 < Z_2 < Z_3$, according to well-known principles.[5] As stated by Eqs. (11), (13), and (14), thin plates with characteristic impedances that are higher than the load impedance are well approximated as masses at low frequency. The three layers of the HF section can therefore be lumped into a single mass component with

$$L_{1,3} = \frac{2\pi}{\omega_{\mathrm{H}}} \sum_{i=1}^{3} \nu_i Z_i,$$

where $\nu_i = d_i \lambda_{\mathrm{H}}^{-1}$ is the fractional thickness of each layer, referenced to the wavelength at the centre of the HF band, λ_{H}.

The impedance loading the first isolation layer has a large inductance relative to the inductance of the first isolation layer. The normalized load impedance magnitude, α, is large, and the phase is close to 90°. For this case, Eq. (12)

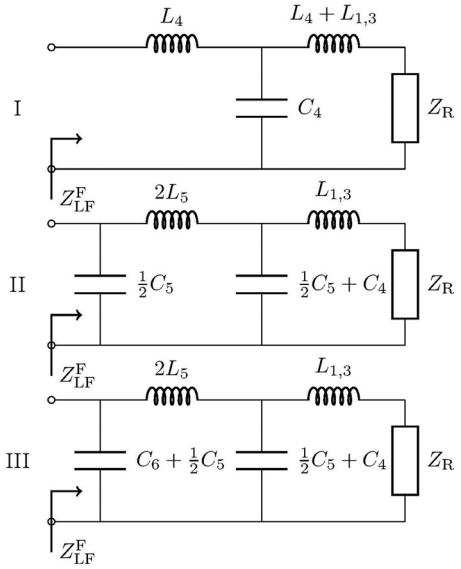

FIG. 8. The circuit models used to analyze the loading conditions of the LF transducer with the isolation section configurations from Fig. 5.

and Fig. 4 show that the first isolation layer can be modeled by a single capacitance with

$$C_4 = \frac{2\pi}{\omega_H}\frac{\nu_4}{Z_4}.$$

However, when considering a single isolation layer, it is straightforward to include the mass component of the layer in a T-model, and it is therefore included in this case, as seen in Fig. 8(I).

Due to its high characteristic impedance it is tempting to approximate the second isolation layer as a mass. However, as shown by Fig. 9, the impedance loading the second isolation layer does not always satisfy Eq. (13). The approximation would neglect the influence of the layer on the resonance which occurs due to the mass–spring interaction

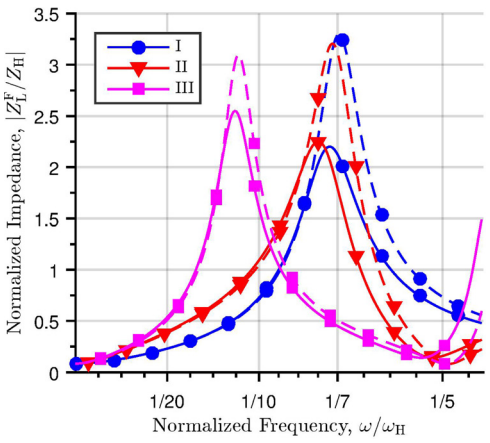

FIG. 9. (Color online) Magnitude of the LF acoustic loading impedance for three isolation section configurations. The impedances are normalized to the characteristic impedance of the HF layer. The solid lines show the result calculated using the distributed model, whereas the dashed lines show the result using lumped parameters. Parameters for each case are (I) $Z_4 = 2.34$ MRayl, $\nu_4 = 0.25$, (II) $Z_4 = 2.34$ MRayl, $Z_5 = 44.5$ MRayl, $\nu_4 = \nu_5 = 0.25$, (III) $Z_4 = 2.34$ MRayl, $Z_5 = 44.5$ MRayl, $Z_6 = 2.34$ MRayl, $\nu_4 = \nu_5 = \nu_6 = 0.25$.

of the first isolation layer and the HF section. In the following it will therefore be modeled as a Π-filter. The resulting circuit model is shown in Fig. 8(II).

The loading condition of the third isolation layer is dominated at low frequency by the inductance of the second isolation layer and the HF section. Again, Eq. (12) and Fig. 4 show that it can be modeled with a single capacitance so that

$$C_6 = \frac{2\pi}{\omega_H}\frac{\nu_6}{Z_6},$$

and the resulting circuit model is shown in Fig. 8(III).

One can expect from the circuit models in Fig. 8 that the isolation section functions as a low pass filter with a resonance and Q-factor given by the characteristic impedance and thickness of each layer. It is therefore to be expected that the expression for the acoustic impedance loading the LF transducer, $Z^F_L(\omega)$, is the ratio of two complex polynomial functions. The loading impedance can be analyzed simply by determining the location of the first pole of the undamped impedance. At resonance, the loading impedance will be real, and the LF transducer will be efficiently matched to the load, depending on the Q-factor of the resonance.

To increase readability, the following quantities are defined and will be used in later expressions:

$$\begin{aligned}
Z_{i,j} &= \sum_{n=i}^{j}\nu_n Z_n, & Y_i &= \frac{\nu_i}{Z_i},\\
\zeta^k_{i,j} &= 1 + \frac{\nu_l Z_l}{2Z_{j,k}}, & \Upsilon^j_i &= 1 + \frac{Y_j}{2Y_i},\\
\zeta_R &= \frac{\nu_5 Z_5}{Z_{1,3}}, & \Upsilon_R &= \frac{Y_6}{Y_4}\frac{\Upsilon^5_6}{\Upsilon^5_4},\\
\zeta_T &= 1 + \zeta_R, & \Upsilon_T &= Y_4\Upsilon^5_4 Y_6\Upsilon^5_6,\\
\omega_a &= 2\pi\omega/\omega_H.
\end{aligned} \tag{20}$$

$Z_{i,j}$ describes the total mass of layers i through j. Y_i is the compliance of a layer i. $\zeta^k_{i,j}$ is a term containing the ratio between the mass of layer k to the total mass of layers i through j. When layer k has a negligible mass in comparison to layers i through j, $\zeta^k_{i,j} \to 1$. Υ^j_i is a term containing the ratio between the compliances of layers i and j. ζ_R is the ratio of mass between the second isolation layer and the HF section of the stack, to which ζ_T is also related. Υ_R is approximately the ratio of compliances between the first and third isolation layers, modified by the compliance of the second isolation layer. Υ_T is the product of these compliances. ω_a is the normalized angular frequency.

2. Loading impedance

a. Configuration I. Using the lumped parameter model, the loading conditions of the LF section can be analyzed though circuit analysis of the circuits in Fig. 8. Starting with isolation section configuration I, the loading impedance of the LF section of the stack can be expressed as

$$Z_L^F(\omega) = \frac{Z_R\left(1-\omega_a^2\nu_4^2/2\right) + \jmath\omega_a Z_{1,4}}{1-\omega_a^2 Z_{1,3}\zeta_{1,3}^4 Y_4 + \jmath\omega_a Z_R Y_4}. \tag{21}$$

When the isolation layer is optimized for HF performance, $\nu_4 Z_4 \ll Z_{1,4}$, and $Z_{LF}^F(\omega)$ has two distinct resonances. By evaluating the minimum of the denominator in Eq. (21), the damped parallel resonance, $\hat{\omega}_4$, with purely resistive load is found at

$$\hat{\omega}_4 \approx \frac{\omega_H}{2\pi}\sqrt{\frac{1}{Z_{1,3}\zeta_{1,3}^4}\left(\frac{1}{Y_4} - \frac{2Z_R^2}{Z_{1,3}\zeta_{1,3}^4}\right)}. \tag{22}$$

Omitting the characteristic acoustic impedance of the loading material, $Z_R = 0$, the undamped resonance is found at

$$\omega_4 \approx \frac{\omega_H/(2\pi)}{\sqrt{Y_4 Z_{1,3}\zeta_{1,3}^4}}. \tag{23}$$

An example of the loading impedance in Eq. (21) is shown in Fig. 9 alongside the impedance calculated with a distributed model. As expected, the impedance increases from $\omega_a = 0$ to a peak at ω_4, before decreasing. The lumped model follows the distributed model closely at lower frequency, but overestimates the impedance magnitude around the peak. This deviation is caused by regarding the layers of the HF section as a pure mass. Including the compliance for each of these layers rectifies the overestimation problem, but complicates the mathematical analysis.

The location of the resonance in the loading impedance is dependent on the compliance of the isolation layer, Y_4, and the total mass of the HF section, $Z_{1,3}$. The dependency of ω_4 on ν_4 is illustrated in Fig. 10. As shown in Fig. 6 (CI) and (PI), the first isolation layer should be a quarter of the HF wavelength in order to minimize spurious transmit pulses. The parameters that define the loading impedance in Eq. (21) are therefore fixed according to the HF section of the probe, and the resonance frequency ω_4 is also given by HF design considerations.

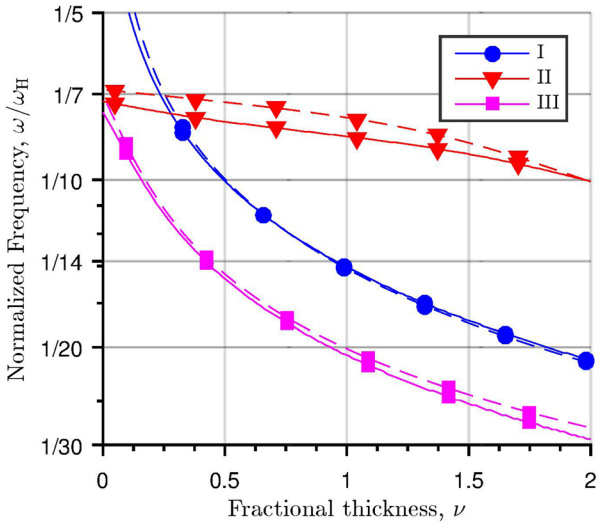

FIG. 10. (Color online) Resonance frequency of the LF load impedance as a function of fractional thickness, for three configurations. For each configuration, the thickness of the rear layer is varied, while the thickness of each other layer is kept constant at $\nu = 0.25$. The resonance is calculated using lumped (dashed) and distributed (solid) models. The parameters for each case are equal to those in Fig. 6.

b. Configuration II. Configuration II is modeled by the middle circuit in Fig. 8. By circuit analysis, the loading impedance can be expressed as

$$\begin{aligned} Z_{\mathrm{L}}^{\mathrm{F}}(\omega) = &\left[Z_{\mathrm{R}}\left(1-\omega_a^2\nu_5 Z_5 Y_4 \Upsilon_4^5\right)\right. \\ &\left. + \jmath\omega_a Z_{1,3}\left(\zeta_{\mathrm{T}} - \omega_a^2\nu_5 Z_5 Y_4 \Upsilon_4^5\right)\right] \\ &\times \left[1 + \jmath\omega_a Z_{\mathrm{R}} Y_4 \Upsilon_4^5\left(1 + \frac{Y_5}{2Y_4\Upsilon_4^5} - \omega_a^2\nu_5^2/2\right)\right. \\ &\left. - \omega_a^2 Z_{1,3} Y_4 \Upsilon_4^5\left(1 + \frac{Y_5\zeta_{\mathrm{T}}}{2Y_4\Upsilon_4^5} - \omega_a^2\nu_5^2/2\right)\right]^{-1}, \end{aligned} \tag{24}$$

where several definitions from Eq. (20) have been utilized. From Fig. 6, minimizing spurious HF transmission requires $\nu_5 \approx 0.25$. Additionally, when ω_a is small, the term $\omega_a^2\nu_5^2/2 \ll 1$. In this case the denominator is equivalent to the denominator of an LC-circuit, where the equivalent capacitance is proportional to the sum of the compliances $Y_4 + Y_5$, and the inductance is proportional to the modified sum of the mass of the second isolation layer and the HF section, $Z_{1,3} + 2\nu_5 Z_5(1 + Y_4/Y_5)$. The impedance resonance frequency is therefore approximately governed by the combined compliance of the two isolation layers, and the combined masses of the HF section and the second isolation layer. The full expression for the resonance frequency of the loading impedance in Eq. (24) is

$$\begin{aligned} \omega_5 = &\frac{\omega_{\mathrm{H}}/(2\pi)}{\sqrt{2\nu_5 Z_5 Y_4 \Upsilon_4^5}}\left[\zeta_{\mathrm{T}} + 1 + 2\frac{Y_4}{Y_5}\right. \\ &\left. - \sqrt{\left(\zeta_{\mathrm{T}} + 1 + 2\frac{Y_4}{Y_5}\right)^2 - \zeta_{\mathrm{R}}\left(1 + 2\frac{Y_4}{Y_5}\right)}\right]^{1/2}, \end{aligned} \tag{25}$$

which reduces to

$$\hat{\omega}_5 = \frac{\omega_{\mathrm{H}}/(2\pi)}{\sqrt{\nu_5 Z_5 Y_4 \Upsilon_4^5}}\sqrt{\zeta_{\mathrm{T}} + 1 + 2\frac{Y_4}{Y_5}}, \tag{26}$$

by neglecting the term $\omega_a^2\nu_5^2/2$. Introducing the second isolation layer causes the impedance resonance to shift downwards in frequency from ω_4 by a factor $1 + Y_5(1+\zeta_{\mathrm{T}})/2Y_4$. The shift is given by the ratios ζ_{R}, from Eq. (20); and the ratio of the compliance in the two isolation layers, Y_4/Y_5. The null of the numerator also shifts downwards in frequency, in particular, when Z_5 is large. This causes asymmetry in the impedance resonance peak, as seen in Fig. 9,

which shows an example of the loading impedance. The lumped model follows the distributed model closely below resonance, where it overestimates the impedance. This error occurs due to the omission of the compliance of the layers in the HF section.

The variation in the location of the impedance resonance with ν_5 is shown for a fixed $\nu_4 = 0.25$ in Fig. 10. For large Z_5 the resonance is relatively constant with ν_5, up to a certain thickness, where it starts to decrease as the thickness increases. As Z_5 is decreased, ω_5 becomes linearly decreasing with ν_5. Further decreases in Z_5 decreases the mass and stiffness of the layer, and the two isolation layers combine to act as a single spring.

Again, Fig. 6 (CII) and (PII) show that the spurious HF transmissions are minimized when the fractional thickness of the second isolation layer is $\nu_5 \sim 0.25$. Selecting the layer thickness to optimize HF performance therefore limits the choice for ν_4 and ν_5, and Z_4 and Z_5. With $\nu_4 = 0.25$, and a large ratio Z_5/Z_4, the difference $\omega_5 - \omega_4$ is not large, and mainly depends on ζ_R according to Eq. (26).

c. Configuration III. Configuration III is modeled by the bottom circuit in Fig. 8. The LF loading impedance is found from circuit analysis and can be written as

$$Z_L^F(\omega) = \left[Z_R\left(1 - \omega_a^2 \nu_5 Z_5 Y_4 \Upsilon_4^5\right) + \jmath\omega_a Z_{1,3}\left(\zeta_T - \omega_a^2 \nu_5 Z_5 Y_4 \Upsilon_4^5\right)\right] \times \left[1 + \jmath\omega_a \nu_5 Z_5 Z_R \Upsilon_T\left(\frac{1+\Upsilon_R}{\nu_5 Z_5 Y_6 \Upsilon_6^5} - \omega_a^2\right) - \omega_a^2 \nu_5 Z_5 Z_{1,3} \Upsilon_T\left(\frac{1+\zeta_T \Upsilon_R}{\nu_5 Z_5 Y_6 \Upsilon_6^5} - \omega_a^2\right)\right]^{-1}, \quad (27)$$

where the parameter Υ_T, defined in Eq. (20), denotes the product of the model capacitances from Fig. 8. Υ_R from Eq. (20) denotes the ratio between the capacitances. The numerator is no different than in Eq. (24), but the denominator is modified by the addition of the third isolation layer, meaning that the location of the resonance peak is moved. The distance between the maximum and minimum of the impedance is increased, and the resonant peak becomes more symmetric, similar to the peak of configuration I. An example is shown in Fig. 9, where there is good agreement between the lumped and distributed models except at the resonance. The undamped resonance frequency of Eq. (27) can be found at

$$\omega_6 = \frac{\omega_H/(2\pi)}{\sqrt{2\nu_5 Z_5 Y_6 \Upsilon_6^5}}\left[1 + \zeta_T \Upsilon_R - \sqrt{\left(1+\zeta_T \Upsilon_R\right)^2 - 4\zeta_R \Upsilon_R}\right]^{1/2}. \quad (28)$$

The location of the resonance is dependent on the mass of the second isolation layer, $\nu_5 Z_5$; the ratio between the mass of the second isolation layer and the HF section, ζ_R, ζ_T; the compliance of the third isolation layer, Y_6; the ratio between the compliance of the second and third isolation layers Υ_6^5; and the ratio of the compliance of the first and third isolation layer, Υ_R.

Equations (27) and (28) are involved expressions as they must account for the case where $Y_6 < Y_4$. However, by letting $Y_6 > Y_4$, e.g., $\nu_6 > \nu_4$, the expressions simplify since the resonant behavior of Y_4 and $Z_{1,3}$ can be neglected. In this case the impedance loading the third isolation layer can be approximated by the two inductances, L_5 and $L_{1,3}$ in Fig. 8, and the impedance is simply governed by the mass–spring interaction between the compliance of the third isolation layer and the total mass of the layers in front. Equation (28) is approximated by

$$\hat{\omega}_6 = \frac{\omega_H/(2\pi)}{\sqrt{\nu_5 Z_5 Y_6 \Upsilon_6^5}}\left(\frac{\zeta_R}{\zeta_T}\right)^{1/2} = \frac{\omega_H/(2\pi)}{\sqrt{(\nu_5 Z_5 + Z_{1,3}) Y_6 \Upsilon_6^5}}. \quad (29)$$

The variation in Eq. (28) with ν_6 is shown for a fixed $\nu_4 = \nu_5 = 0.25$ in Fig. 10. The behavior is similar to that of varying ν_4 in configuration I, but the resonance is lower due to the added mass of the heavy second isolation layer. This confirms the dominance of the mass–spring interaction of Eq. (29), for $Y_6 > Y_4$. As ν_6 increases, the model error increases due to the omission of the mass of the third isolation layer and the compliance of the layers in the HF section.

With configuration III, Fig. 6 (CIII) and (PIII) show that the HF performance is not sensitive to the selection of the thickness of the third isolation layer. Y_6 can therefore be selected by varying the fractional thickness of the third isolation layer, ν_6, without significant loss in HF performance, meaning that the HF backing impedance optimization and the LF loading impedance optimization are decoupled.

IV. CONCLUSIONS

The HF-to-LF ratio in a dual-band ultrasound probe is important in SURF imaging. It is a challenge to design a probe with a specific HF-to-LF ratio while maintaining the performance of the HF and LF transducers in the probe. This paper shows how a stack design using three layers of material in between the HF and LF transducers tackles this challenge. It shows that the layers in the isolation should have alternating low and high characteristic impedance in order to minimize spurious HF transmission. The low-loss simulations in Fig. 6 show that spurious HF transmission amplitudes are reduced to –60 to –55 dB relative to the amplitude of the main HF transmission pulse.

With a single, low impedance layer in the isolation section, the HF-to-LF ratio is typically ~6:1, as shown by Fig.

10. Adjusting the HF-to-LF ratio by varying the thickness of the single isolation layer is detrimental to HF performance, as shown by Fig. 6. In theory, this ratio can be increased indefinitely by using three isolation layers, as shown by Eqs. (28) and (29) and Fig. 10. However, the authors hypothesize that very large ratios, $\chi_R > 20{:}1$, are more efficiently obtained by increasing the number of layers in the isolation section, since very thick layers with low impedance may introduce a large amount of absorption. Furthermore, increasing the thickness of the third isolation layer causes the magnitude of the loading impedance peak to decrease to a point where the LF transducer is no longer efficiently matched to the load.

Equations (21), (24), and (27) show that the loading condition of the LF transducer follows closed form expressions which are useful for design purposes. In certain cases these expressions reduce to simple equations describing a mass–spring interaction between layers with low characteristic impedance and layers with high characteristic impedance, as shown by Eqs. (23), (26), and (29).

The addition of a high impedance material in the acoustic stack may open new possibilities for controlling the temperature of the probe. Copper is a material with high thermal conductivity, large characteristic impedance, and large sound speed. Consequently, the thickness of a copper layer is relatively large when used in the isolation section of the probe. The combination of the relatively large thickness and large thermal conduction makes the copper layer suitable as a heat sink. Efficient use of such a heat sink would increase the ability of a probe to withstand high power transmissions.

It has not escaped the authors' notice that the isolation section may also be included in single-band probes. Using two isolation layers between the backing and the transducer in a single-band probe would enable cooling of such a probe. The authors recommend that the possibilities for probe cooling with the proposed design should be investigated, particularly in light of recent developments in ultrasound mediated drug delivery.

ACKNOWLEDGMENTS

The authors extend their gratitude to Ole Martin Brende and Stian Solberg for proofreading the manuscript.

APPENDIX: SIMULATION PARAMETERS

The parameters in Table I are used to generate the examples of Figs. 6, 7, 9, and 10. Note that the isolation layer thicknesses are given for $\nu_k = 0.25$, but these are varied in the various examples. See the relevant figure caption for more details on the parameters in each example.

TABLE I. Parameters used to generate examples. HF and LF piezo have piezoelectric constant $h = 14.3 \times 10^8$ V/m and relative dielectric constant $\epsilon_r = 10^3$.

Layer	#	Z (MRayl)	c (m/s)	Q	l (μm)
Backing	8	2.50	2500	50	
LF piezo	7	20.00	3500	50	3111.50
Isolation 3	6	2.34	2500	50	69.44
Isolation 2	5	44.50	4500	50	125.00
Isolation 1	4	2.34	2500	50	69.44
HF piezo	3	20.00	3500	50	172.86
Matching 2	2	6.87	2500	50	69.44
Matching 1	1	2.36	2500	50	69.44
Load	0	1.65	1540	50	

[1]B. A. J. Angelsen and R. Hansen, "7A-1 SURF imaging—A new method for ultrasound contrast agent imaging," in *IEEE Ultrasonics Symposium* (2007), pp. 531–541.
[2]R. Hansen, S.-E. Måsøy, T. F. Johansen, and B. A J. Angelsen, "Utilizing dual frequency band transmit pulse complexes in medical ultrasound imaging," J. Acoust. Soc. Am. **127**, 579–587 (2010).
[3]R. Hansen and B. A J. Angelsen, "SURF imaging for contrast agent detection," IEEE Trans. Ultrason., Ferroelectr. Freq. Control **56**, 280–290 (2009).
[4]S. Eggen, S.-M. Fagerland, Ý. Mørch, R. Hansen, K. Søvik, S. Berg, H. Furu, A. D. Bøhn, M. B. Lilledahl, A. Angelsen, B. Angelsen, and C. de Lange Davies, "Ultrasound-enhanced drug delivery in prostate cancer xenografts by nanoparticles stabilizing microbubbles," J. Controlled Release **187**, 39–49 (2014).
[5]C. Desilets, J. Fraser, and G. Kino, "The design of efficient broad-band piezoelectric transducers," IEEE Trans. Sonics Ultrason. **25**, 115–125 (1978).
[6]T. Azuma, M. Ogihara, J. Kubota, A. Sasaki, S. Umemura, and H. Furuhata, "Dual-frequency ultrasound imaging and therapeutic bilaminar array using frequency selective isolation layer," IEEE Trans. Ultrason., Ferroelectr., Freq. Control **57**, 1211–1224 (2010).
[7]S. de Fraguier, J.-F. Gelly, L. Wolnerman, and O. Lannuzel, "A novel acoustic design for dual frequency transducers resulting in separate bandpass for color flow mapping (CFM)," in *IEEE Symposium on Ultrasonics* (1990).
[8]J. M. Rau, "Dual frequency band ultrasound for suppression of multiple scattering," Ph.D. dissertation, Norwegian University of Science and Technology, Trondheim, Norway, 2013.
[9]O. M. Brende and B. Angelsen, "Adaptive reverberation noise delay estimation for reverberation suppression in dual band ultrasound imaging," J. Acoust. Soc. Am. **138**, 3341–3351 (2015).
[10]R. Hansen, "New techniques for detection of ultrasound contrast agents," Ph.D. dissertation, Norwegian University of Science and Technology, Trondheim, Norway, 2003.
[11]Norwegian Research Council, "Improved imaging and quantitative identification of acoustic tissue properties with dual band ultrasound pulse complexes" https://www.forskningsradet.no/prosjektbanken/#!/project/254633/no (Last viewed16 January 2017).
[12]O. F. Myhre, J. Kvam, and B. A. J. Angelsen, "Dual frequency transducer design for suppression of multiple scattering," in *IEEE International Ultrasonics Symposium (IUS)* (2016).
[13]B. A J. Angelsen, "Plane waves in a linear elastic medium," in *Ultrasound Imaging—Waves, Signals and Signal Processing* (Emantec AS, Bugges Vei 4B, 7051 Trondheim, Norway, 2000), vol. 1, Chap. 2, pp. 2.1–2.43.
[14]C. H. Sherman and J. L. Butler, "Transducer models," in *Transducers and Arrays for Underwater Sound*, 1st ed. (Springer Science+Business Media, New York, 2007), Chap. 7, pp. 320–375.
[15]W. P. Mason, *Electromechanical Transducers and Wave Filters*, 2nd ed. (Van Nostrand Reinhold Inc., New York, 1948).
[16]B. A. J. Angelsen, T. F. Johansen, R. Hansen, S.-E. Måsøy, and P. Näsholm, "Dual frequency band transducer arrays," U.S. patent 7,727,156 (26 July 2006).